Bioorganic Chemistry 167 (2025) 109260

Contents lists available at ScienceDirect

Bioorganic Chemistry

journal homepage: www.elsevier.com/locate/bioorg

ProTide-enabled antibody-drug conjugates: A novel platform for the targeted delivery of phosphorylated drugs

Sofia Siciliano [a], Clizia Bernardi [a], Federica Finetti [a], Asia Guerrini [a], Maria Chiara Monti [b,c], Elva Morretta [b,c], Elena Petricci [a], Federica Poggialini [a], Giulia Romagnoli [a], Maurizio Taddei [a], Lorenza Trabalzini [a], Giorgia Vinciarelli [a], Demetra Zambardino [a], Elena Cini [a,*]

[a] Dipartimento di Biotecnologie, Chimica e Farmacia, Università degli Studi di Siena, Via A. Moro 2, 53100 Siena, Italy
[b] Dipartimento di Farmacia, Università di Napoli Federico II, Via Montesano 49, 80131, Napoli, Italy
[c] Dipartimento di Farmacia, Università di Salerno, Via Giovanni Paolo II, 84084, Fisciano, Salerno, Italy

ARTICLE INFO

Keywords:
ProTide
Phosphorylated drug
Drug delivery
Bioconjugates
ADCs
Gemcitabine
Linker

ABSTRACT

Herein, we report the first integration of ProTide technology with antibody-drug conjugates (ADCs) to create a novel platform that enables the targeted delivery of active, phosphorylated drugs. Our ADCs contain a specially designed ProTide linker that exploits the ProTide enzymatic activation pathway to release monophosphorylated nucleoside analogues directly into target cells. Using gemcitabine as a model drug conjugated to trastuzumab lysines, we demonstrated good antiproliferative activity in HER2-positive cancer cell lines (SKBR3 and MIA PaCa-2) compared to the unconjugated antibody and existing ProTide formulations. The lead compound achieved IC_{50} values of 0.25 μM (SKBR3) and 0.19 μM (MIA PaCa-2), which represent a significant improvement over current therapies. Mechanistic studies confirmed the successful enzymatic release of the drug and the maintenance of the internalization properties of the antibody. This platform fulfils the requirement to deliver phosphorylated drugs while minimising resistance and systemic toxicity. Beyond nucleoside analogues, this approach opens up new possibilities for the targeted delivery of other phosphate-containing therapeutics, potentially expanding the scope of ADC technology.

1. Introduction

Phosphate and phosphonate drugs have broad clinical applications, serving as anticancer (i.e. Etoposide phosphate, Fludarabine phosphate), antiviral (i.e. Fostemsavir, Fosamprenavir), and anti-inflammatory agents (i.e. Hydrocortisone Sodium Phosphate), as well as nutritional supplements (i.e. Pyridoxal phosphate, D-glucosamine-6-phosphate) (Scheme 1A) [1,2]. Being negatively charged, these molecules often suffer from poor membrane permeability, thus affecting their efficacy and requiring high doses to obtain the expected therapeutic effect. In the case of Nucleoside Analogues (NAs), a non-phosphorylated nucleoside prodrug can be used (e.g., AZT, Ribavirin, Galidesivir), which requires in situ activation by mono-, di-, or tri-phosphorylation [3,4]. This crucial process for the activity of NA, it is often disabled in tumor resistant cells or in resistant viral strains, where down-regulation of phosphorylating enzymes is frequently observed [5].

The conjugation of NAs with aptamers [6], DNA nanocarriers [7], knotting proteins [8], and RGD sequences [9] have been reported with the aim to overcome resistance but has been met with poor practical applications in therapy. Discovered in 2008 by Chris McGuigan and Jan Balzarini, the "ProTide" technology represents the most efficient and innovative approach to improve the efficacy and overcome resistance of Nucleoside Analogues (NAs) and other phosphate-containing drugs (i.e. saccharides) [10–12]. Several drugs based on ProTide technology have been approved by the Food and Drug Administration (FDA) such as Sofosbuvir [13], Tenofovir alafenamide [14], and Remdesivir [15], and a plethora of ProTide-based prodrugs are in the pipelines of numerous pharma companies for applications as anticancer or antiviral drugs beyond NAs, as it is well demonstrated that phosphoramidates of non-nucleoside substrates share the same activation pathways of their NAs counterparts (Scheme 1B) [16].

ProTide technology takes advantage of the direct use of a masked monophosphorylated NA or non-NA drug, where the primary alcohol of the drug is phosphorylated and one of the phosphate oxygens is

* Corresponding author.
E-mail address: elena.cini@unisi.it (E. Cini).

https://doi.org/10.1016/j.bioorg.2025.109260
Received 3 July 2025; Received in revised form 29 October 2025; Accepted 15 November 2025
Available online 16 November 2025

functionalized with a properly designed aryl moiety. The phosphate is transformed into the corresponding phosphoramidate through its functionalization with an α-amino acid ester. The prodrug obtained usually shows a higher passive penetration of cell membranes and a higher activity with respect to the non-phosphorylated drug or the corresponding monophosphorylated one [11]. Once the ProTide-based drug is internalized, the cleavage of the ester moiety occurs by esterase or carboxypeptidase-type enzymes and the hydrolysis triggers a cyclization to form an oxazaphospholidin-2-one that is rapidly hydrolyzed to a phosphoarmidate metabolite (metabolite B and metabolite C in Scheme 1, respectively). Phosphoramidase-type enzymes cleave the P—N bond to release the final monophosphorylated drug inside the cell, which is then rapidly converted into the active tri-phosphorylated derivative (Scheme 2) [11].

Despite their pharmacokinetic improvements, the targeted delivery of phosphate drugs to specific tissues, cells or sites, it is still a hot topic in medicinal chemistry. This goal may be reached by connecting the drug to a targeting moiety such as a monoclonal Antibody (mAb), due to the ability of the mAb to selectively target a cell expressing its specific antigen [17]. If the mAb is covalently connected with a drug through a linker, the targeted system is called Antibody-Drug Conjugate (ADC). The ADC is supposed to be stable in the systemic circulation but, after reaching its target, the drug can be released through a trigger mechanism controlled by chemical or enzymatic stimuli present in the targeted site [18]. The presence of elevated ROS concentrations, variation in redox potential, or pH values between diseased and healthy tissues are efficient chemical tools for drug release. Alternatively, release can be induced by enzymes overexpressed or present exclusively in the targeted cells, such as cathepsin B [19], penicillin-G-amidase [20], neutrophil-secreted elastase [21], β-glucuronidase [22,23] or β-galactosidase [24].

2. Results and discussion

2.1. Design, synthesis and characterization of antibody-ProTide conjugates

Building on our interest in ADCs [25–28], we explored the possibility of combining the ProTide and ADC strategies to enable the targeted delivery of phosphate drugs. This approach aims to allow the rapid triphosphorylation of the drugs in target tissues, enhancing their cell permeability, reduce their side effects and reduce their systemic and off-target toxicity. Phosphinates have been previously employed as warheads for cysteine selective bioconjugation [29] and different phosphates have been exploited to link and release glucocorticoid payloads from ADCs [30].

We report here on an innovative linker for ADCs that can utilize the activation pathway of ProTide technology to release active phosphorylated drugs into target cells (Scheme 3). Our preliminary communication was prompted by an ongoing study using self-immolative phosphoramidates for the release of hydroxy-containing drugs [31].

We chose gemcitabine as a model for our ProTide-based targeted drugs because it is a nucleoside analogue with significant clinical value due to its strong antitumour activity, particularly against pancreatic cancer, and it is one of the most studied nucleoside analogues in terms of reactivity, biological activity, and side effects [32]. Its clinical application has long been hampered by limitations such as a short half-life, rapid metabolic degradation, poor tumor tissue penetration, resistance, and dose-dependent toxicity. Many attempts have been made to overcome these issues, including nanoformulations and prodrugs such as the extensively investigated ProTide Acelarin (NUC-1031, Scheme 1), which achieved high response rates and acceptable tolerability in patients with solid tumours and reached phase 3 clinical trials [33–36].

We designed the ProTide linker with an alkyne on the aryl protection of the phosphate to allow the introduction of a chain ending with a carboxylic acid for connection to the antibody lysines. According to the role of amino acids in the release of monophosphorylated gemcitabine [33], (L)-alanine benzyl and isopropyl derivatives were prepared. Thus, 3-ethynylphenol **1** was reacted with $POCl_3$ at low temperature to give the intermediate phosphorodichloridate **2** that, after filtration to remove the ammonium salts and concentration under an inert atmosphere, was immediately quenched with (L)-alanine benzyl ester (**3a**) or isopropyl ester (**3b**) (Scheme 4). The formation of phosphoramidochloridates **4a** or **4b** was verified by ES-MS of the crude reaction mixture. Due to the instability of these intermediates, after rapid filtration through a silica pad under argon, they were immediately reacted with tri-Boc protected gemcitabine (**5**) in the presence of *t*BuMgCl to give compounds **6a** and **6b** in 55% and 64% yields, respectively (Scheme 4). The coupling between the nucleoside and the phosphorochloridate yields potentially a mixture of diastereoisomers due to phosphorus stereogenic centre. In some cases, the two ProTide diastereoisomers exhibit similar potency, in other cases, such as for *S*p- and *R*p-diastereoisomer of Sofosbuvir they may have different rates of metabolism and hence varying potency [33,37–38]. The gemcitabine ProTide NUC-1301 (Acelarin) is one of the cases in which *S*p-and *R*p-diastereoisomers exhibit similar potency [33], we then proceeded with synthesis even though a nearly 1:1 mixture of the two diastereomers (See SI for NMR) was obtained for both **6a** and **6b**.

Phosphoramidates **6a** and **6b** were subjected to a Cu catalyzed Huisgen reaction with 6-azidohexanoic acid in the presence of Cu(II) acetate and sodium ascorbate in DMF/water, providing the desired

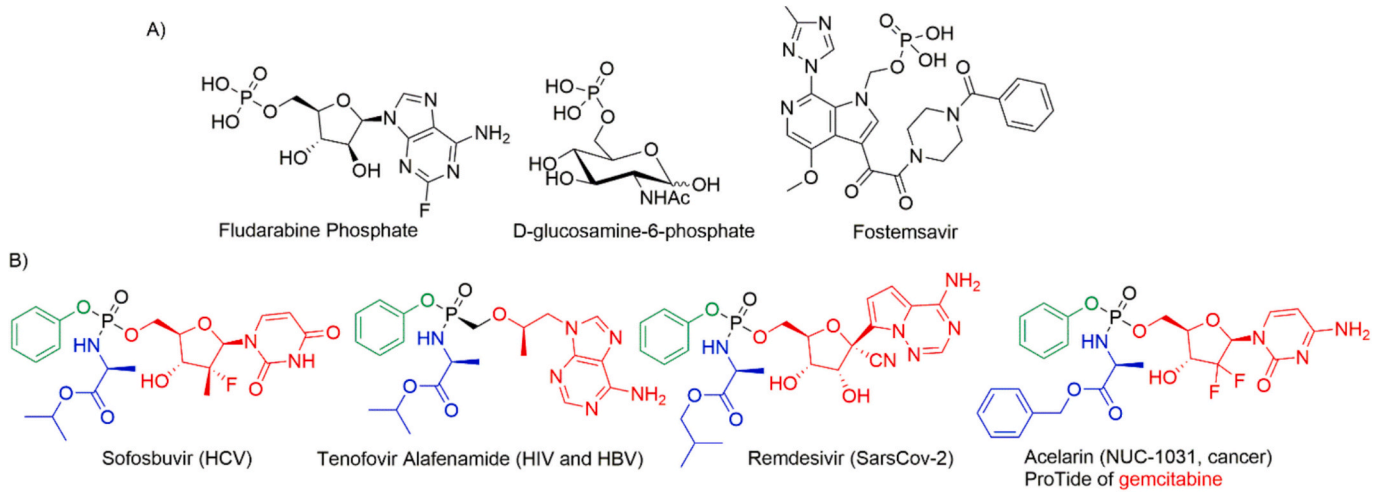

Scheme 1. Examples of Phosphonate drugs (A) and ProTides (B)

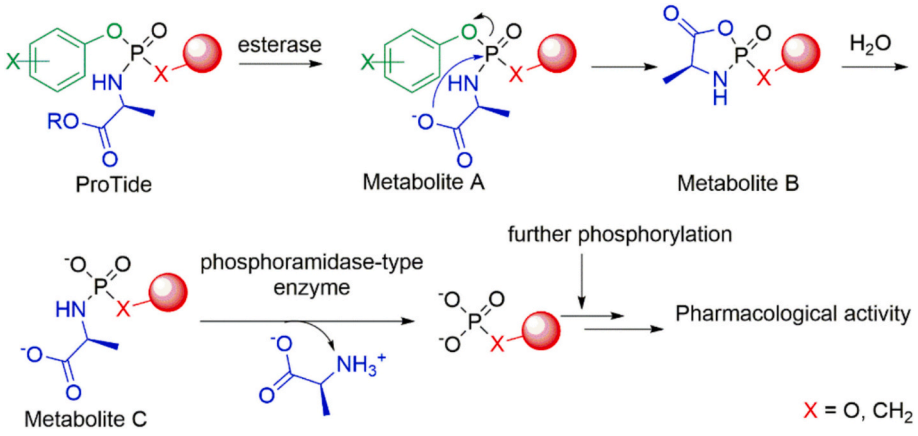

Scheme 2. Activation pathway of ProTides

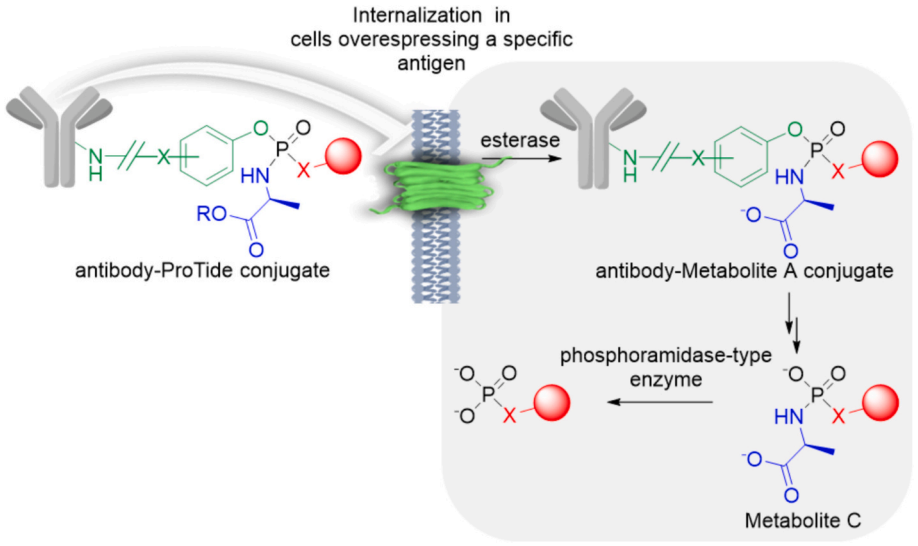

Scheme 3. Proposed mechanism of the selective activation of antibody-ProTide conjugates.

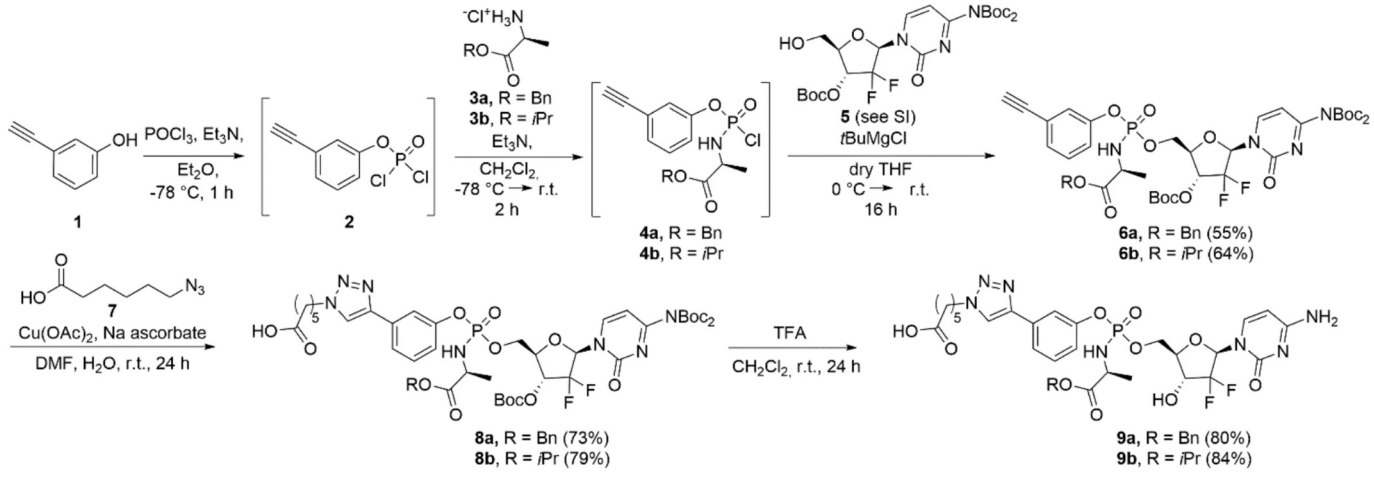

Scheme 4. Preparation of the ProTide cargos

compounds **8a** and **8b** in good yields that were deprotected using TFA (Scheme 4).

Compounds **9a** and **9b** were tested in human plasma at 37 °C for 24 h, showing high stability (see SI). Cargos **9a** and **9b** were then transformed into the corresponding NHS-esters and reacted with trastuzumab, a mAb targeting the HER2 receptor. Conjugation through the stable amide bond afforded ADCs **10a** and **10b** (Scheme 5).

Purification of **10a** and **10b** was carried out by dialysis, and the drug

antibody ratio (DAR) was determined by MALDI analysis (see SI).

Furthermore, a UHPLC-MS analysis of **10a** and **10b** was performed, after extensive disulfide reduction by DTT (Fig. 1). The spectra of the reduced **10a** and **10b** showed both the light and heavy chains of ADCs: the light chains gave better MS spectra with respect to heavy ones because of their low MW, as expected. As shown in the multi charged spectra reported in Fig. 1A and B and Table S1, the light chain of each ADC occurs in its unmodified form (MW = 23,438.3 ± 1.3 Da), covalently linked to one molecule of **9a** or **9b** (MW = 24,181.5 ± 0.7 Da and of 24,132.4 ± 1.2 Da, respectively), to two molecules of **9a** or **9b** (MW = 24,925.3 ± 1.1 Da and of 24,829.6 ± 1.1 Da, respectively) and to three molecules of **9a** (MW = 25,668.8 ± 1.9 Da). The mass increment measured for each molecule of **9a** covalently linked to a lysine residue is around 743 Da, compatible with the MW of **9a** (761.24 Da) and the loss of one molecule of water due to the amide formation. The increment measured for **9b** is around 695 Da, compatible with the MW of **9b** (713.24 Da) and the loss of one molecule of water. In parallel, as shown in the multicharged spectra reported in Fig. 1C and D and Table S1, the heavy chain of ADCs occurs in its unmodified form (MW = 50,592.3 ± 0.8 Da) and covalently linked to one molecule of **9a** or **9b** (MW = 51,333.5 ± 2.7 Da and of 51,288.6 ± 0.8 Da, respectively).

These results are consistent with MALDI analyses, pointing out slightly more extensive conjugation for **10a** with respect to **10b**.

2.2. Evaluation of metabolic pathway

To verify our initial hypothesis that the enzymatic release of the monophosphorylated gemcitabine occurs when the molecule is linked to an antibody, we designed an experiment where ADC **10a** and **10b** were incubated with carboxypeptidase Y, an esterase with high structural and functional homology to lysosomal Catepsin A, responsible for ProTide metabolism [39], and the formed metabolite C (reference compound was prepared according to Ref. 39) was quantified by UHPLC/MRM-MS over the time. ADC **10a** and **10b** were diluted in PBS and treated with carboxypeptidase Y to monitor the metabolic conversion, performing UHPLC/MRM-MS runs every 20 min and monitoring the area of the peak relative to the formation of metabolite C (MRM transition of the precursor ion at *m/z* of 415.2 to daughter ion at m/z of 246.0). Both for **10a** and **10b**, a time-dependent release of metabolite C was observed, but with different rates (Fig. 2A and B). Indeed, metabolite C release from

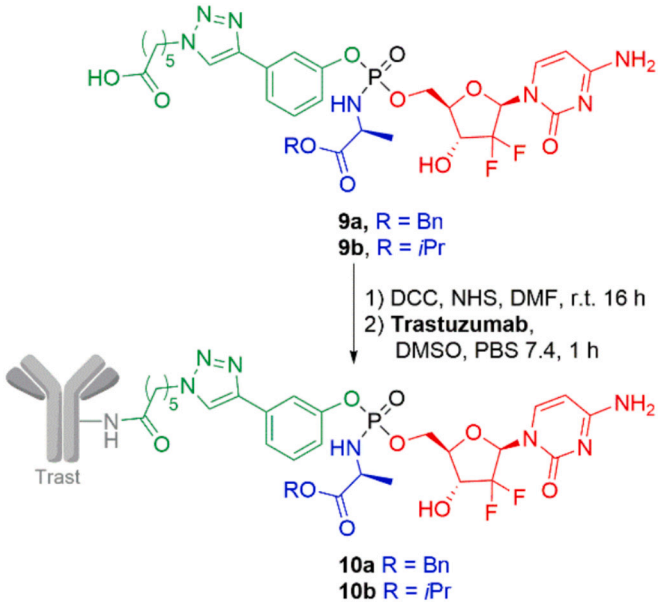

Scheme 5. Conjugation of ProTides with trastuzumab (trast). DAR determined by MALDI analysis: **10a** DAR = 4.6; **10b** DAR = 3.8.

10a is faster, and the plateau is reached after 60 min of incubation with the enzyme, while the release from **10b** is slower. These data agree with observations done on unconjugated gemcitabine ProTides that showed a higher activity of the benzyl ester [33]. The release of metabolite C from the unconjugated ProTide is well established, however the metabolism of one of our linker-payloads (**9a**), as an opportune control, has also been monitored by UHPLC/MRM-MS (Fig. 2C). We have designed an experiment where compound **9a** was incubated the carboxypeptidase Y and the consumption of the precursor together with the formation of metabolite C were both quantified by UHPLC/MRM-MS over the time. Compound **9a** was diluted in PBS at the concentration of 1 μM and treated with carboxypeptidase Y (compound **9a**:CBY at ratio of 1:20 *w/w*) to monitor the metabolic conversion, performing UHPLC/MRM-MS runs every 40 min and monitoring the area of the peak relative to metabolite C (MRM transition of the precursor ion at *m/z* of 415.2 to daughter ion at m/z of 246.0) and compound **9a** (MRM transition of the precursor ion at m/z of 762.4 to daughter ion at m/z of 246.0).

A similar time-dependent release of metabolite C was observed on the unconjugated ProTide compared to the corresponding ADC as reported in the Fig. 2.

2.3. In vitro internalization and proliferation assays on HER2 positive cancer cell lines

To study the biological activity of ADCs **10a** and **10b** we used two different cellular models both overexpressing HER2 receptor, as MIA PaCa-2 (human pancreatic adenocarcinoma) and SKBR3 (human breast carcinoma) cell lines [40–41]. The binding of the ADCs with the receptor was evaluated by measuring the internalization rate of HER2 after drug exposure by immunofluorescence analysis. Results show that HER2 receptors undergo internalization upon binding to trastuzumab and the ADCs. The extent of internalization was comparable to that observed with unconjugated trastuzumab (Fig. 3A and B), indicating that both ADCs effectively bind to the HER2 receptors present on the cell surface.

To investigate the antiproliferative activity of the conjugates **10a** and **10b**, SKBR3 and MIA PaCa-2 cell lines were treated for 72 h with increasing concentrations of ADCs, trastuzumab and NUC-1031 (gemcitabine ProTide, Scheme 1) (Fig. 4A and B). Treatment with both conjugates reduced cell viability (Fig. 4), reaching maximal activity at 125 and 250 nM. Compound **10a** is more effective than **10b** in both cell lines. In order to confirm the selectivity and the specificity of ADCs, both compounds were evaluated in HER2-negative cell lines (MCF7 and MDA-MB-231) as well as in non-tumoral cell lines (normal human dermal fibroblast, NHDF), in which they exhibited no antiproliferative activity (see S14 and S15 SI). This result is consistent with the in vitro release of metabolite C from ADCs **10a** and **10b** upon treatment with carboxypeptidase Y (Fig. 2) and with higher activity of the unconjugated gemcitabine benzyl-ProTide compared to other esters [33]. Moreover, compound **10a** demonstrated greater antiproliferative activity than NUC-1031, with the most pronounced effect observed in MIA PaCa-2 cells (Fig. 4).

IC_{50} values (Table 1) and the percentage of inhibition at 250 nm (Table 2) further highlight the potency of conjugate **10a** compared to **10b** and NUC-1031 and Trastuzumab on both SKBR3 and MIA PaCa-2 cells.

Conjugation to trastuzumab cysteines via Michael addition to the maleimide derivative of compound **9a** was also investigated (see SI for the synthesis). As shown in Fig. 5, compound **10c** significantly reduced cell viability on MIA PaCa-2 cells although with a lower activity compared to compound **10a.**

We also aimed to evaluate the impact on cell viability of non-targeted ADCs but the conjugation to lysines of human IgG1 isotype control monoclonal antibody was unsuccessful while the conjugation to cysteines resulted in a good drug to antibody ratio (see SI). We obtained compound **10d** that resulted inactive in the biological assay (Fig. 5), confirming the selectivity of our ADCs.

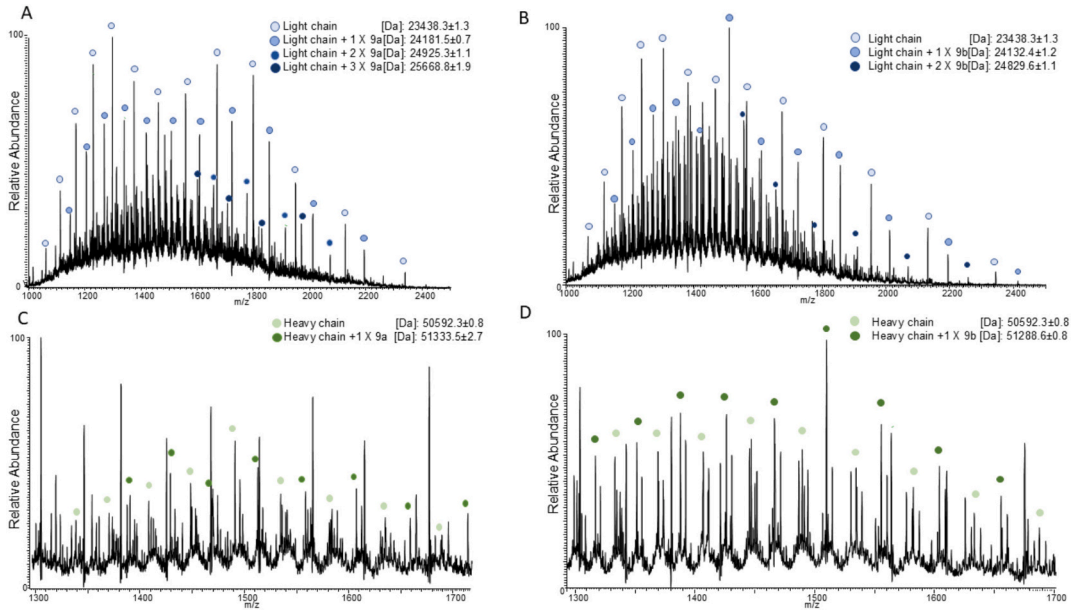

Fig. 1. Multi-charged ions ESI-MS spectra of **10a** (A, C) and **10b** (B, D). The samples have been treated with DTT to reduce inter-chains disulfide bridges; the light and heavy chains of **10a** and **10b** were separated by UPLC and their MS spectra have been reported (**10a** light chain Panel A, **10a** heavy chain Panel C; **10b** light chain Panel B, **10b** heavy chain Panel D). Multicharged ions belonging to each species are indicated by coloured circles and the corresponding molecular weights were reported in Dalton together with the errors.

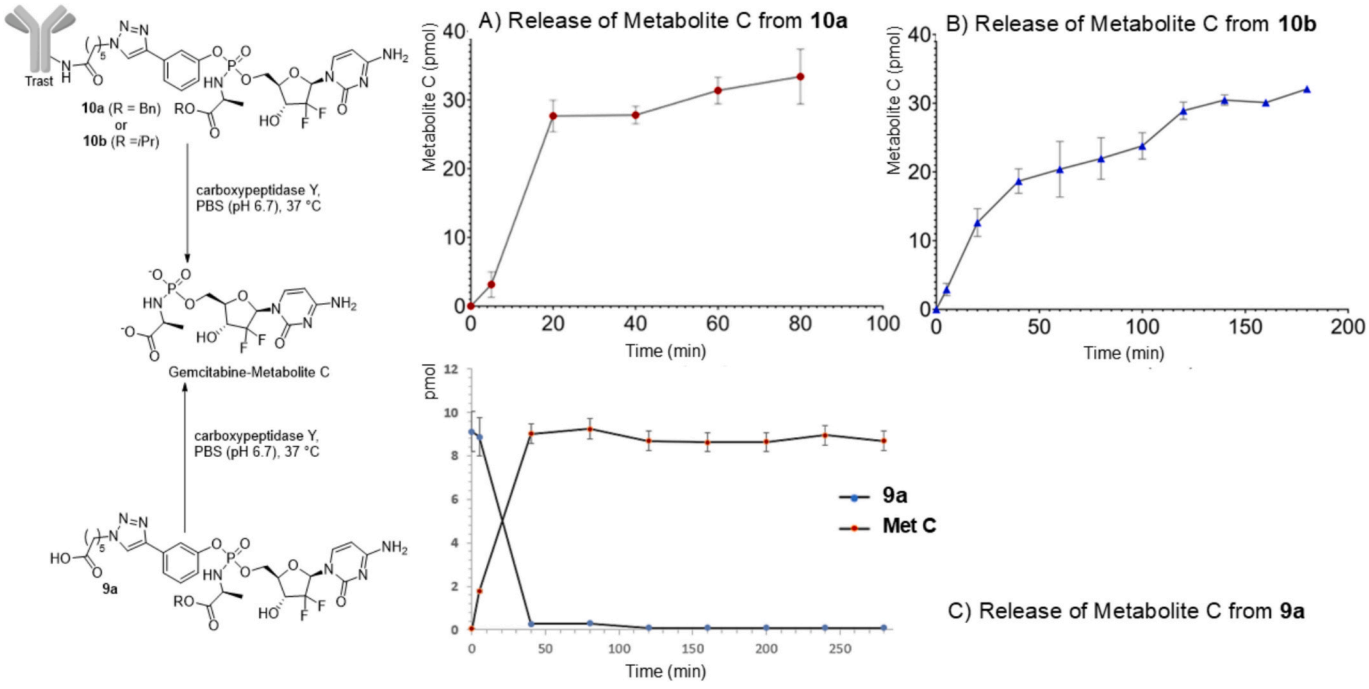

Fig. 2. Release of picomoles of Metabolite C from **10a** (A) and **10b** (B) over time after carboxypeptidase Y digestion compared to release of unconjugated ProTide **9a** (C).

The aim of this work was to prove that is possible to apply ProTide technology to build an ADC that selectively releases a phosphorylated drug into cells overexpressing the antigen recognized by the monoclonal antibody. We used gemcitabine as a proof of concept, however, as we employed ProTide chemistry to synthesize the ProTide core of our ADC, and since ProTide technology has been applied to many phosphorylated drugs [11], our ProTide-based ADC can reasonably be extended to all existing ProTide applications and beyond. Simply modifying the key components of ProTide (the amino acid ester and hydroxy- or methylene-containing drugs) enables application to different phosphorylated drugs, while changing the monoclonal antibody allows antibody-ProTide activity to be directed towards other specific targets (not exclusively tumours). Moreover, since ADCs belong to the class of biotechnology drugs, the approval process for their commercialisation is faster than that for new small molecules and this could result in potential new clinical or translational challenges for phosphorylated drugs.

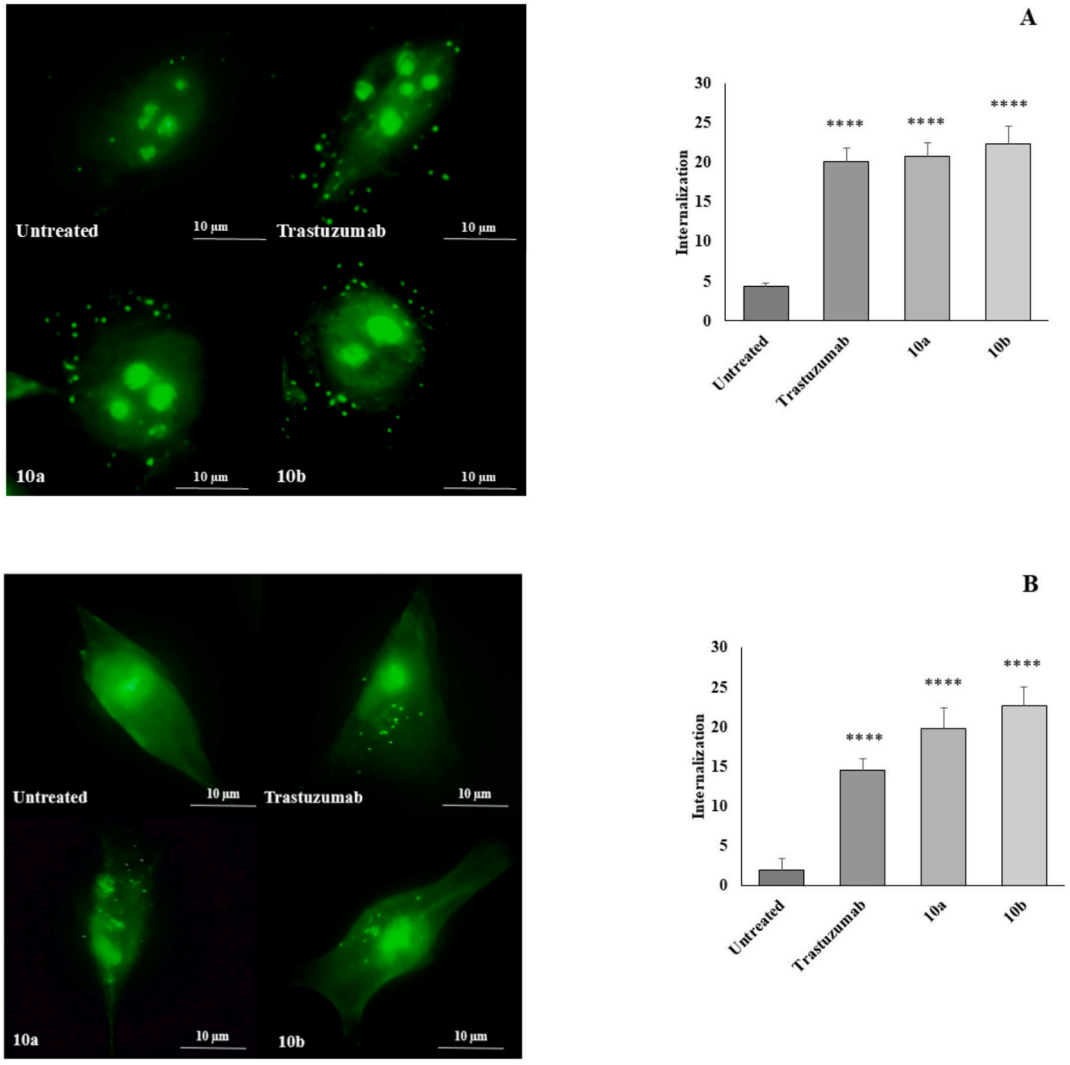

Fig. 3. Internalization of new ADCs **10a** and **10b**, as compared to trastuzumab in SKBR3 (A) and in MIA PaCa-2 (B). Cells were treated with trastuzumab (10 μg/mL) and the conjugates **10a** and **10b** (10 μg/mL) for 2 h in 0.1% serum and HER2 localization was analyzed by immunofluorescence analysis. Images are representative of 3 different experiments. The graphs illustrate the quantitative analysis of the internalization process, calculated as the number of internalized clusters per cell.

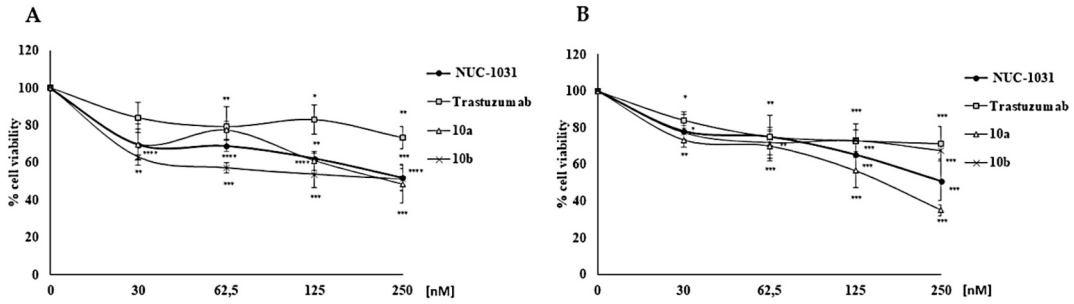

Fig. 4. Cell viability. Cancer cell survival was evaluated by MTT test. SKBR3 (A) and MIA PaCa-2 (B). Cells were exposed to increasing concentrations of conjugate **10a** and **10b**, NUC-1031, or trastuzumab. Data are expressed as a percentage of cell viability. $*p < 0.05$ vs. basal; $**p < 0.01$ vs. basal and $***p < 0.001$ vs. basal.

3. Conclusions

We developed a new class of ADCs able to deliver phosphorylated active drugs inside the target cells, exploiting the release/activation pathway of ProTide technology. The linker was stable in plasma and the ADCs charged with gemcitabine released the phosphorylated drug in vitro. The reduction in cell viability by compounds **10a** and **10b** observed in the MTT assay suggests that the proposed drug release mechanism of our ADCs occurs also in tumor cell models expressing high levels of HER2. The absence of detectable activity of our compounds in receptor-negative cancer cells, as well as in non-malignant cells, supports their potential selectivity and favourable safety profile, as expected for this type of targeted drugs. Their higher activity compared to NUC-1031 demonstrates that our esterase-responsive drug delivery system can be crucial to expand the payload scope in ADCs as it can be versatilely applied to other NAs and to non-nucleoside monophosphate

Table 1
IC_{50} values of compounds **10a** and **10b**, trastuzumab and NUC-1031 against tumor SKBR3 and MIA PaCa-2 cell lines (μM). Table 1 is representative of five independent experiments. Statistical analysis was performed using one-way ANOVA (GraphPad Prism 8.4.3). ** $p < 0.01$; * $p < 0.05$.

Compds	SKBR3	MIA PaCa-2
NUC-1031	0.43 ± 0.07 **	0.22 ± 0.01 **
Trastuzumab	2.14 ± 0,12 *	2.45 ± 0.182 *
10a	0.25 ± 0.03 **	0.19 ± 0.07 *
10b	0.25 ± 0.05 *	0.52 ± 0.04 *

Table 2
Percentage of inhibition at 250 nm in SBBR3 and MIA PaCa-2 cells. Table 2 is representative of five independent experiments. Statistical analysis was performed using one-way ANOVA (GraphPad Prism 8.4.3). ****$p < 0.0001$; *** $p < 0.001$.

Compds	SKBR3	MIA PaCa-2
NUC-1031	48,1% ± 7,2 ****	48,1% ± 10,9 ***
Trastuzumab	26,42% ± 6,2 **	28,71% ± 9,4 ***
10a	51,52% ± 10,2 ***	64,98% ± 3,1 ***
10b	48,78% ± 5,6 ***	32,44% ± 4,6 ***

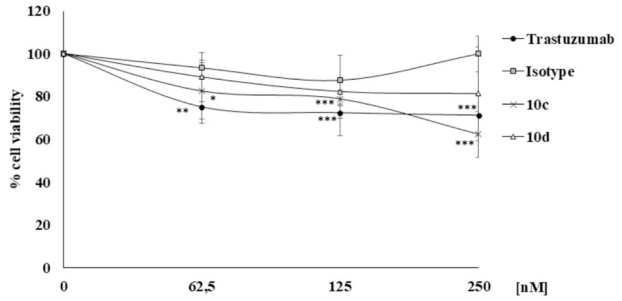

Fig. 5. Cell viability. Cancer cell survival was evaluated by MTT test. MIA PaCa-2 cells were exposed to increasing concentrations of conjugate **10c** and **10d** or trastuzumab. Data are expressed as a percentage of cell viability. *$p < 0.05$ vs. basal; **$p < 0.01$ vs. basal and ***$p < 0.001$ vs. basal.

and monophosphonate drugs. These new ADCs are able not only to deliver the NAs and other active compounds to the target tissue but also to overcome the main resistance mechanisms that are related to the phosphorylation step.

4. Experimental part

4.1. Chemistry general

All reagents were used as purchased from commercial suppliers without further purification. The reactions were carried out in oven dried or flamed vessels. Solvents were dried and purified by conventional methods prior use or, if available, purchased in anhydrous form. Flash column chromatography was performed with Merck silica gel 60, 0.040–0.063 mm (230–400 mesh). Merck aluminum backed plates precoated with silica gel 60 (UV254) were used for analytical thin layer chromatography and were visualized by staining with a $KMnO_4$ solution. NMR spectra were recorded at 25 °C and 400 or 600 MHz for ^1H and 101 or 151 MHz (JMOD) for ^{13}C Brücker Advance NMR spectrometers were used. Spectra were recorded in $CDCl_3$ and CD_3OD, under these conditions exchangeable protons were never observed. The solvent is specified for each spectrum. Splitting patterns are designated as s, singlet; d, doublet; t, triplet; q, quartet; m, multiplet; bs, broad singlet. Chemical shifts (d) are given in ppm relative to the resonance of their respective residual solvent peaks. High- and low-resolution mass spectroscopy analyses were recorded by electrospray ionization with a mass spectrometer Q-exactive Plus. ES-MS analysis was performed by Agilent 1100 LC/MSD VL system (G1946C) (Agilent Technologies. Palo Alto. CA) constituted by a vacuum solvent degassing unit, a binary high-pressure gradient pump, an 1100 series UV detector, and an 1100 MSD model VL benchtop mass spectrometer. The Agilent 1100 series mass spectra detection (MSD) single-quadrupole instrument was equipped with the orthogonal spray API-ES (Agilent Technologies. Palo Alto. CA). Nitrogen was used as nebulizing and drying gas (flow 9 mL/min, temperature 350 °C). The analysis was performed at a flow rate of 0.4 mL/min. Spectra were acquired over the scan range *m/z* 100–1500 both in positive and negative mode (fragmentor 70).

4.2. Procedure for the preparation of target compounds

4.2.1. Gemcitabine phosphoramidate *6a*

3-Ethynylphenol **1** (77 μL, 0.72 mmol) was solubilized in dry Et_2O (2 mL) in a Schlenk tube under Ar atmosphere. The solution was cooled at −78 °C and dry $POCl_3$ (70 μL, 0.72 mmol) in dry Et_2O (1 mL) and dry Et_3N (100 μL, 0.72 mmol) in dry Et_2O (1 mL) were slowly added with the formation of a yellowish precipitate. The mixture was stirred at r. t. for 1 h. The crude was filtered under Ar on a silica gel pad and washed with Et_2O (2 × 10 mL). The solvent was removed under vacuum at 25 °C. Crude phosphodichloride **2** was used for the next step without further purification. Compound **2** (0.72 mmol) was solubilized in dry CH_2Cl_2 (2 mL) under Ar and esterified amino acid (benzyl L-alanine hydrochloride **3a** (154 mg, 0.72 mmol) or isopropyl L-alanine hydrochloride **3b** (121 mg, 0.72 mmol) was added; the solution was cooled at −78 °C and Et_3N (200 μL, 1.44 mmol) in CH_2Cl_2 (1 mL) was added dropwise. The suspension was stirred at −78 °C for 1 h, heated at r. t. and stirred for additional 30′. The solvent was removed under vacuum, under Ar at 25 °C; Et_2O (30 mL) was added to the resulting crude oil, and the mixture was filtered on a silica gel pad under Ar to remove triethylammonium salts. Et_2O was removed under vacuum at 25 °C and a yellow-green oil was obtained. Crude product **4a** or **4b** was used in the next step without further purification. To a solution of nucleoside **5** (100 mg, 0.18 mmol) in dry THF (3 mL), *t*BuMgCl 1 M in Me-THF (220 μL, 0.22 mmol) was slowly added at 0 °C under Ar and the solution stirred for 10′. To this solution, phosphoramide **4a** or **4b** (0.54 mmol) in dry THF (2 mL) was added. The mixture was stirred at r. t. for 3 h. Silica gel (350 mg) was added, and the solvent removed under vacuum. The crude was immediately purified by flash chromatography on silica gel, gradient MeOH in CH_2Cl_2 0–5%. The product was obtained in 55% yield (88 mg). **ES-MS:** *m/z* 905 $[M + H]^+$, 927 $[M + Na]^+$. **HRMS** (ES^+) $C_{42}H_{51}F_2N_4O_{14}PNa$ 927.3006; found 927.3008. **^1H** and **^{13}C** refer to the mixture of diastereoisomers.

^1H NMR (400 MHz, $CDCl_3$) δ 7.90–7.59 (m, 1H), 7.31–7.01 (m, 10H), 6.39–6.29 (m, 1H), 5.17–5.06 (m, 3H), 4.40–3.44 (m, 5H), 3.07–3.05 (m, 1H), 1.52 (s, 18H), 1.47 (s, 9H), 1.39–1.32 (m, 3H). **^{13}C NMR**: (100 MHz, $CDCl_3$) δ 173.08, 172.94, 162.80, 153.90, 153.74, 151.84, 151.49, 151.42, 150.13, 149.31, 149.26, 149.24, 144.19, 144.09, 143.96, 135.30, 135.15, 129.80, 129.72, 129.55, 129.05, 128.99, 128.63, 128.61, 128.54, 128.49, 128.43, 128.29, 128.25, 128.20, 123.86, 123.73, 123.59, 123.51, 121.15, 120.88, 120.83, 123.79, 96.79, 85.16, 84.74, 84.54, 83.23, 82.66, 82.33, 79.59, 78.44, 78.36, 77.96, 77.05, 67.41, 67.17, 60.11, 50.45, 50.13, 27.66 (6C), 27.53 (3C), 20.83.

4.2.2. Gemcitabine phosphoramidate *6b*

The product was obtained in 64% yield (100 mg) following the procedure described for **6a**. **ES-MS:** m/z 857 $[M + H]^+$, 879 $[M + Na]^+$. **HRMS** (ES^+) calcd. For $C_{38}H_{51}F_2N_4O_{14}PNa$ 879.3006; found 879.3009. **^1H** and **^{13}C** refer to the mixture of diastereoisomers.**^1H NMR** (600 MHz, $CDCl_3$) δ 7.90–7.65 (m, 1H), 7.35–7.06 (m, 5H), 6.41–6.31 (m, 1H), 5.23–5.02 (m, 2H), 4.48–4.31 (m, 3H), 4.17–3.71 (m, 2H), 3.10 (s, 1H), 1.56 (s, 18H), 1.51 (s, 11H), 1.40–1.37 (m, 3H), 1.24–1.22 (m, 4H). **^{13}C NMR** (151 MHz, $CDCl_3$) δ 172.59, 171.26, 162.83, 153.89, 153.77,

151.94, 151.50, 149.33, 149.26, 143.94, 129.84, 129.76, 129.07, 129.02, 123.88, 123.72, 123.62, 122.01, 121.00, 120.87, 120.84, 120.34, 96.81, 85.24, 85.18, 84.79, 84.71, 82.35, 79.45, 78.40, 78.32, 78.06, 72.47, 71.69, 69.53, 64.36, 60.24, 50.39, 27.68 (6C), 27.54 (3C), 21.69, 21.62, 21.00.

4.2.3. Protected gemcitabine ProTide *8a*

Compound **6a** (70 mg, 0.08 mmol) and 6-azidohexanoic acid **7** (9 mg, 0.06 mmol) were solubilized in DMF (3 mL) under Ar and the solution was degassed with three cycles of Ar/vacuum. To this solution, a freshly prepared mixture of $Cu(OAc)_2$ (4 mg, 0.02 mmol) and Na ascorbate (8 mg, 0.04 mmol) in water (1.5 mL), previously degassed by argon/vacuum cycles, was added. The reaction mixture was stirred at r. t. for 24 h. The solvent was evaporated, and the crude purified by silica gel flash chromatography with gradient MeOH in CH_2Cl_2 0–10% to provide 47 mg (73%) of **8a**. **ES-MS:** *m/z* 1062 $[M + H]^+$, 1084 $[M + Na]^+$. HRMS (ES^+) calcd. For $C_{48}H_{62}F_2N_7O_{16}PNa$ 1084.3857; found 1084.3854. **^{1}H** and **^{13}C** refer to the mixture of diastereoisomers. **^{1}H NMR** (600 MHz, $CDCl_3$) δ 7.83–7.82 (m, 1H), 7.70–7.69 (m, 1H), 7.48–7.00 (m, 10H), 6.41–6.37 (m, 1H), 5.23–4.97 (m, 4H), 4.70–4.29 (m, 6H), 2.40 (m, 2H), 1.98 (m, 2H), 1.77 (m, 2H), 1.56 (s, 18H), 1.51 (s, 9H), 1.42–1.34 (m, 5H). **^{13}C NMR** (151 MHz, $CDCl_3$) δ 176.67, 172.83, 162.84, 153.88, 151.51, 151.28, 149.27, 138.74, 138.17, 135.15, 134.97, 133.92, 130.92, 130.59, 128.66, 128.58, 128.57, 128.43, 128.32, 128.12, 118.48, 117.86, 117.66, 96.82, 96.81, 85.25, 84.81, 78.06, 72.66, 67.47, 67.35, 67.26, 67.15, 64.80, 64.64, 50.26, 50.22, 33.46, 29.70, 28.75, 27.68 (6C), 27.55(3C), 24.59, 22.60, 20.58.

Protected gemcitabine ProTide **8b** was obtained with 79% of yield (46 mg) following the above describe procedure starting from compound **6b** (50 mg, 0.06 mmol). **ES-MS:** *m/z* 1014 $[M + H]^+$, 1036 $[M + Na]^+$, 1012 $[M-H]^-$. HRMS (ES^+) calcd. For $C_{44}H_{62}F_2N_7O_{16}PNa$ 1036.3857; found 1036.3859. **^{1}H** and **^{13}C** refer to the mixture of diastereoisomers. **^{1}H NMR** (600 MHz, $CDCl_3$) δ 8.26–8.16 (m, 2H), 7.91–7.70 (m, 4H), 7.06–6.96 (m, 1H), 6.44–6.39 (m, 1H), 5.30–5.02 (m, 3H), 4.91–4.83 (m, 1H), 4.68–4.37 (m, 4H), 1.94–1.71 (m, 6H), 1.56–1.51 (m, 27H), 1.39–1.23 (m, 11H). **^{13}C NMR** (151 MHz, $CDCl_3$) δ 176.64, 172.57, 162.85, 153.90, 151.50, 150.66, 150.62, 150.08, 149.27, 144.18, 140.72, 132.68, 130.46, 122.00, 120.35, 118.93, 116.78, 111.31, 96.82, 96.79, 85.25, 84.84, 78.17, 78.14, 72.73, 69.52, 64.69, 50.27, 48.56, 33.43, 33.37, 29.71, 28.88, 27.68 (6C), 27.55 (3C), 24.56, 22.62, 21.50, 20.95.

4.2.4. ProTide gemcitabine cargo *9a*

Compound **8a** (50 mg, 0.05 mmol) was solubilized in CH_2Cl_2 (2 mL) and trifluoracetic acid (108 μL, 1.41 mmol) was added dropwise. The solution was stirred at r. t. for 16 h. The excess of TFA was removed under vacuum co-evaporating with CH_2Cl_2 three times. The crude was purified by silica gel flash chromatography with gradient MeOH in CH_2Cl_2 0–15% to provide **9a** (30 mg), 80% yield **ES-MS:** *m/z* 762 $[M + H]^+$, 784 $[M + Na]^+$, 760 $[M-H]^-$. **HRMS** (ES^+) calcd. For $C_{33}H_{38}F_2N_7O_{10}PNa$ 784.2284 found 784.2287. **^{1}H** and **^{13}C** refer to the mixture of diastereoisomers. **^{1}H NMR** (600 MHz, MeOD) δ 8.32–8.29 (2 x s, 1H), 7.71–7.63 (m, 2H), 7.55–7.49 (m, 1H), 7.43–7.39 (m, 1H), 7.33–7.27 (m, 5H), 7.21–7.17 (m, 1H), 6.21 (m, 1H), 5.82 (m, 1H), 5.13–5.10 (m, 2H), 4.48–4.43 (m, 3H), 4.39–4.32 (m, 1H), 4.22–4.19 (m, 1H), 4.05–4.04 (m, 2H), 2.28 (m, 2H), 1.97–1.96 (m, 2H), 1.66–1.64 (m, 2H), 1.39–1.36 (m, 5H). **^{13}C NMR** (151 MHz, MeOD) δ 173.39, 173.22, 166.08, 156.20, 151.21, 146.35, 141.13, 135.78, 132.32, 130.09, 130.06, 128.19, 127.93, 127.81, 123.76, 122.03, 121.98, 121.34, 119.79, 117.21, 78.92, 69.74, 69.67, 66.63, 66.61, 64.47, 64.30, 50.42, 50.31, 49.94, 29.54, 25.60, 24.05, 19.04, 18.88.

ProTide gemcitabine Cargo **9b** was obtained following the previously described procedure in 84% yield. **ES-MS:** *m/z* 714 $[M + H]^+$, 736 $[M + Na]^+$,712 $[M-H]^-$. **HRMS** (ES^+) calcd. For $C_{29}H_{38}F_2N_7O_{10}PNa$ 736.2284; found 736.2282. **^{1}H** and **^{13}C** refer to the mixture of diastereoisomers. **^{1}H NMR** (600 MHz, MeOD) δ 8.35–8.32 (2 x s, 1H), 7.73–7.65 (m, 2H), 7.58–7.43 (m, 2H), 7.26–7.22 (m, 1H), 6.26–6.24 (m, 1H), 5.87–5.83 (m, 1H), 5.01–4.96 (m, 1H), 4.57–4.54 (m, 1H), 4.47–4.36 (m, 3H), 4.25–4.20 (m, 1H), 4.13–4.09 (m, 1H), 3.98–3.93 (m, 1H), 2.28–1.97 (m, 2H), 1.70–1.65 (m, 2H), 1.39–1.36 (m, 5H), 1.29 (m, 2H), 1.23–1.21 (m, 6H). **^{13}C NMR** (151 MHz, MeOD) δ 176.20, 173.00, 172.97, 160.39, 151.21, 150.42, 147.34, 144.08, 143.96, 132.37, 132.33, 130.16, 129.68, 128.65, 123.97, 123.87, 123.42, 123.38, 122.08, 120.91, 120.88, 120.83, 120.80, 119.80, 119.77, 117.21, 79.94, 78.53, 70.46, 69.83, 68.90, 64.36, 50.39, 49.95, 33.23, 29.53, 25.56, 23.94, 20.58, 20.50, 19.12., 18.97.

General procedures for the preparation of ADCs through conjugation via amino groups of lysine residues. **10a** (Trast-NH-**9a**), **10b** (Trast-NH-**9b**).

The proper carboxylic acid (**9a** or **9b**, 0.01 mmol) was dissolved in anhydrous DMF (0.5 mL) in a round bottom flask under N_2 and magnetic stirring. DCC (3 mg, 0.014 mmol) and *N*-hydroxysuccinimide (2 mg, 0.014 mmol) were added to the solution and the mixture stirred at rt. for 16 h. The white solid was removed by filtration and the solvent removed under vacuum, to provide a white solid (MS(ESI): m/z 881 $[M + Na]^+$ for activated **9a**, 833 $[M + Na]^+$ for activated **9b**) that was dissolved in DMSO in order to obtain a 10 mM solution.

A solution of trastuzumab was buffer exchanged using a 10 kDa cutoff dialysis membrane to obtain the antibody dissolved in PBS at pH 7.4 and to remove interfering preservative (glycine). The concentration of the antibodies after dialysis was determined measuring the OD280 and the observed absorbance was divided by 1.35. A 20-fold molar excess of the various NHS ester 10 mM solution was added to the dialyzed antibody solution.

The reaction was incubated at room temperature with gentle continuous mixing and after 1 h quenched with a 20 mM glycine aqueous solution. The final product was dialyzed in pure water at 4 °C using a 10 kDa cutoff membrane to remove the excess of unreacted payload. The DAR was determined by MALDI mass spectrometry (MALDI -TOF/TOF Bruker UltrafleXtreme).

4.3. UHPLC/MS analysis of the ACDs (DTT reduction procedure)

10a or **10b** (1 μM) were incubated with 1,4-dithiothreitol (DTT, 1 mM) for 45 min, at 500 rpm and at 37 °C. Then, 15 μL of each mixture were analyzed through UHPLC-ESI-MS on an Orbitrap Q-Exactive Classic Mass Spectrometer (ThermoFisher Scientific, Bremen, Germany) coupled to an UltiMate 3000 UHPLC system (ThermoFisher Scientific, Bremen, Germany). Proteins elution was achieved with an Aeris Widepore C4 column (3.6 μm, 150 × 2.1 mm, Phenomenex, Torrance, USA), at a flow rate of 0.200 mL/min and with the following gradient: 3 min at 10% B, 3–23 min to 85% B, then held at 95% B for 3 min and re-equilibrated at 10% B for 6 min (A: 0.1% FA in H_2O; B: 0.1% FA in ACN). Full scan MS spectra were acquired with the following settings: scan range 600–3000 *m/z*, full scan automatic gain control (AGC) target 3e6 at 17,500 resolution, and maximum injection time 200 ms.

4.4. UHPLC-MRM-MS analysis of metabolite C release

20 μg of either **10a** or **10b** (1 μM final concentration) were incubated with carboxypeptidase Y (ADCs to protease ratio of 1:3000 *w/*w) in PBS (pH 6.7). The reaction was allowed to proceed at 37 °C for either 80 min (**10a**) or 180 min (**10b**), and metabolite C production was monitored through UHPLC-MRM-MS, repeatedly injecting 10 μL of each reaction mixture, as well as a calibration curve spanning from 10 nM to 10 μM of pure metabolite C [37]. Compound **9a** at 1 μM was incubated with carboxypeptidase Y (Protide to protease ratio of 1:20 w/w) in PBS (pH 6.7). The reaction was allowed to proceed at 37 °C for 280 min, and both compound 9a and metabolite C were monitored through UHPLC-MRM-MS. Compound **9a** was analyzed as follows: precursor ion at *m/z* of 762.4, daughter ion at m/z of 246.00. Samples were analyzed on a Shimadzu Nexera LC system equipped with a Synergi Fusion-RP column

(2.5 μm, 100 Å, 50 × 2 mm; Phenomenex, Torrance, CA, USA) and interfaced with a Sciex 6500 QTRAP MS. Chromatographic separation was achieved at a flow rate of 0.200 mL/min, using the following gradient: 1 min at 2% B, 1–10 min to 70% B, then held at 90% B for 3 min and re-equilibrated at 2% B for a total of 6 min (A: 0.1% FA in H_2O; B: 0.1% FA in ACN). 6500 QTRAP was operated in positive MRM scan mode and metabolite C was analyzed as follows: precursor ion at m/z of 415.24, daughter ion at m/z of 246.00, dwell time of 90 ms, declustering potential of 85 V, entrance potential of 12 V, collision energy of 20 V and collision cell exit potential of 17 V. Analyst software (version 1.6.2, ABSciex, Foster City, CA, USA) was exploited for data acquisition and processing.

4.5. Stability assays

1) DMSO-stock solutions were diluted at r.t. with H_2O or PBS (25 mM, pH 7.4) up to a final concentration of 200 μM. Aliquot samples (50 μL) were taken at fixed time points (time 0 and 24 h) and by UV/LC-MS to monitor the amount of unmodified compound.
2) DMSO-stock solutions at the final concentration of 2 mM were incubated in presence of human plasma (55.7 μg protein/mL) and HEPES buffer (25 mM, 140 mM NaCl, pH 7.4) at 37 °C under shaking. At selected time points (0 and 24 h), 50 μL of the mix solution were added with cold ACN and centrifuged at 5000 rpm for 10 min. The supernatant was removed and analyzed by UV/LC-MS to monitor the amount of unmodified compound.

LC analysis was performed by Agilent 1100 LC/MSD VL system (G1946C) (Agilent Technologies. Palo Alto. CA) constituted by a vacuum solvent degassing unit, a binary high-pressure gradient pump, an 1100 series UV detector, and an 1100 MSD model VL benchtop mass spectrometer. The Agilent 1100 series mass spectra detection (MSD) single-quadrupole instrument was equipped with the orthogonal spray API-ES (Agilent Technologies. Palo Alto. CA). Nitrogen was used as nebulizing and drying gas. Chromatographic separation was performed using a Phenomenex Kinetex EVO C18-100 Å (150 × 4.6 mm, 5 μm particle size) at room temperature and gradient elution with a binary solution; eluent A was H_2O, while eluent B consisted of ACN (both eluents were acidified with FA 0.1%$_{v/v}$). The analysis started with 5% of B for 3 min, then rapidly increased up to 95% of B in 10 min remaining until 19 min; finally, in one minute came back to the initial conditions of 95% of A. The analysis was performed at a flow rate of 0.6 mL/min. UV detection was monitored at 254 nm. Spectra were acquired over the scan range *m/z* 100–1000 both in positive and negative mode.

4.6. Cell culture

MIA PaCa-2, human pancreatic carcinoma cells (ATCC, Rockville, MD, USA) SKBR3, MCF7 and MDA-MB-231, human breast cancer cells (ATCC, Rockville, MD, USA) were cultured in DMEM; with 4500 mg/L glucose (Euroclone) supplemented with 10% FBS, 100 U/mL penicillin/streptomycin, and 4 mM L-glutamine. NDHF, normal dermal human fibroblasts were cultured in FGM-2 medium supplemented with FGM-2 growth supplements and 10% FBS. All cell lines were grown at 37 °C and 5% CO_2.

4.6.1. MTT assay

3.5×10^3 (MIA PaCa-2), 4.5×10^3 (SKBR3) or 2.0×10^3 (NHDF) cells/well were seeded in 96-multiwell plates in medium with 10% FBS (Euroclone), and after adherence were maintained for 24 h in medium containing 0.1% FBS. After 24 h, cells were treated with different concentrations (30, 62.5, 125, and 250 nM) of NUC-1031, trastuzumab, **10a** and **10b** in medium containing 2% FBS. After 72 h, the medium was removed, and cells were incubated for 4 h with fresh medium in the presence of 1.2 mM MTT (3-(4,5-dimethylthiazol-2-yl)-2,5-diphenyltetrazolium bromide) (Sigma-Aldrich). Then, the supernatant of each well was removed and 50 μL of dimethyl sulfoxide was added into the well to dissolve the blue formazan crystals. Cell viability was evaluated by measuring the absorbance at 595 nm using a microplate reader (EnVision, PerkinElmer, Waltham, MA, USA). Data were expressed as a percentage of the basal control.

4.7. Immunofluorescence assay

5.0×10^4 (MIA PaCa-2) or 6.0×10^4 (SKBR3) cells/well were seeded on glass coverslips placed into 24 multi-well plates and maintained in DMEM 10% FBS for 24 h. Cells were treated with trastuzumab, 10a and 10b (250 nM) in medium containing 2% FBS and, after 2 h, fixed in 4% PFA for 20 min. Tryton 0,1% was added for 10 min. After blocking with 3% bovine serum albumin (BSA) for 30 min, cells were stained with the anti-HER2 antibody (1:100, Sigma-Aldrich) overnight at 4 °C. Samples were then incubated with secondary antibody (1:150, anti-mouse conjugated Alexa Fluor 555, Cell Signaling) for 1 h at room temperature. Cells were examined with an ECLIPSE Ts2 microscope and images were obtained with NIS-Elements software (Nikon).

4.8. Statistical analysis

Data were generated from three independent experiments and expressed as mean ± standard deviation (SD). Statistical analysis was performed using one-way ANOVA multiple comparison test; differences in dataset with $p < 0.05$ were considered statistically significant.

CRediT authorship contribution statement

Sofia Siciliano: Investigation, Formal analysis, Data curation. **Clizia Bernardi:** Validation, Methodology, Investigation, Data curation. **Federica Finetti:** Validation, Supervision, Methodology, Data curation, Conceptualization. **Asia Guerrini:** Investigation. **Maria Chiara Monti:** Resources, Methodology, Investigation, Formal analysis, Data curation. **Elva Morretta:** Formal analysis, Data curation. **Elena Petricci:** Writing – original draft, Resources, Methodology, Funding acquisition. **Federica Poggialini:** Formal analysis. **Giulia Romagnoli:** Methodology, Investigation. **Maurizio Taddei:** Resources, Funding acquisition, Conceptualization. **Lorenza Trabalzini:** Supervision, Resources, Methodology. **Giorgia Vinciarelli:** Investigation, Formal analysis. **Demetra Zambardino:** Methodology, Investigation, Formal analysis. **Elena Cini:** Writing – review & editing, Writing – original draft, Supervision, Methodology, Investigation, Data curation, Conceptualization.

Declaration of competing interest

The authors declare that they have no known competing financial interests or personal relationships that could have appeared to influence the work reported in this paper.

Acknowledgements

This work was supported in part by the AIRC (under IG 2017 – ID. 20758 project – P.I. Maurizio Taddei) and PNRR (THE Tuscany Healty Ecosystem, ECS00000017, Spoke 6 and Deconstructing cancer therapy resistance: integration of advanced in vitro, in vivo and in silico models to dissect patient-specific mechanisms of chemo/immunotherapy resistance, identify novel therapeutic vulnerabilities and generate personalized strategies to target relapse-inducing cancer cells, PNRR-MAD-2022-12376183, P.I. Elena Petricci).

Appendix A. Supplementary data

Supplementary data to this article can be found online at https://doi.org/10.1016/j.bioorg.2025.109260.

Data availability

Data will be made available on request.

References

[1] U. Pradere, E.C. Garnier-Amblard, S.J. Coats, F. Amblard, R.F. Schinazi, Synthesis of nucleoside phosphate and phosphonate prodrugs, Chem. Rev. 114 (18) (2014) 9154–9218.

[2] H. Yu, H. Yang, E. Shi, W. Tang, Development and clinical application of phosphorus-containing drugs, Med. Drug Discov. 8 (2020) 100063.

[3] E. De Clercq, G. Li, Approved antiviral drugs over the past 50 years, Clin. Microbiol. Rev. 29 (3) (2016) 695–747.

[4] J. Shelton, X. Lu, J.A. Hollenbaugh, J.H. Cho, F. Amblard, R.F. Schinazi, Metabolism, biochemical actions, and chemical synthesis of anticancer nucleosides, nucleotides, and base analogs, Chem. Rev. 116 (23) (2016) 14379–14455.

[5] Y. Saiki, Y. Yoshino, H. Fujimura, T. Manabe, Y. Kudo, M. Shimada, N. Mano, T. Nakano, Y. Lee, S. Shimizu, S. Oba, S. Fujiwara, H. Shimizu, N. Chen, Z. K. Nezhad, G. Jin, S. Fukushige, M. Sunamura, M. Ishida, F. Motoi, S. Egawa, M. Unno, A. Horii, DCK is frequently inactivated in acquired gemcitabine-resistant human cancer cells, Biochem. Biophys. Res. Commun. 421 (1) (2012) 98–104.

[6] L. Zhu, J. Yang, Y. Ma, X. Zhu, C. Zhang, Aptamers entirely built from therapeutic nucleoside analogues for targeted cancer therapy, J. Am. Chem. Soc. 144 (4) (2022) 1493–1497.

[7] C. Zhang, M. Han, F. Zhang, X. Yang, J. Du, H. Zhang, W. Li, S. Chen, Enhancing antitumor efficacy of nucleoside analog 5-fluorodeoxyuridine on her2-overexpressing breast cancer by affibody-engineered DNA nanoparticle, Int. J. Nanomedicine 15 (2020) 885–900.

[8] N. Cox, J.R. Kintzing, M. Smith, G.A. Grant, J.R. Cochran, Integrin-targeting knottin peptide–drug conjugates are potent inhibitors of tumor cell proliferation, Angew. Chem. Int. Ed. 55 (34) (2016) 9894–9897.

[9] H. Han, Q. Jin, Y. Wang, Y. Chen, J. Ji, The rational design of a gemcitabine prodrug with AIE-based intracellular light-up characteristics for selective suppression of pancreatic cancer cells, Chem. Commun. 51 (98) (2015) 17435–17438.

[10] Y. Mehellou, J. Balzarini, C. McGuigan, Aryloxy phosphoramidate triesters: A technology for delivering monophosphorylated nucleosides and sugars into cells, Chem. Med. Chem. 4 (11) (2009) 1779–1791.

[11] Y. Mehellou, H.S. Rattan, J. Balzarini, The ProTide prodrug technology: From the concept to the clinic, J. Med. Chem. 61 (6) (2018) 2211–2226.

[12] Y. Mehellou, The ProTides boom, Chem. Med. Chem. 11 (11) (2016) 1114–1116.

[13] E. Cini, G. Barreca, L. Carcone, F. Manetti, M. Rasparini, M. Taddei, Stereoselective synthesis of sofosbuvir through nucleoside phosphorylation controlled by kinetic resolution, Eur. J. Org. Chem. (2018) 2622–2628.

[14] L.M. Childs-Kean, E.F. Egelund, J. Jourjy, Tenofovir alafenamide for the treatment of chronic hepatitis B monoinfection, Pharmacotherapy 38 (10) (2018) 1051–1057.

[15] Y. Wang, D. Zhang, G. Du, R. Du, J. Zhao, Y. Jin, S. Fu, L. Gao, Z. Cheng, Q. Lu, Y. Hu, G. Luo, K. Wang, Y. Lu, H. Li, S. Wang, S. Ruan, C. Yang, C. Mei, Y. Wang, D. Ding, F. Wu, X. Tang, X. Ye, Y. Ye, B. Liu, J. Yang, W. Yin, A. Wang, G. Fan, F. Zhou, Z. Liu, X. Gu, J. Xu, L. Shang, Y. Zhang, L. Cao, T. Guo, Y. Wan, H. Qin, Y. Jiang, T. Jaki, F.G. Hayden, P.W. Horby, B. Cao, C. Wang, Remdesivir in adults with severe COVID-19: A randomised, double-blind, placebo-controlled multicentre trial, Lancet 395 (10236) (2020) 1569–1578.

[16] A.S. Alanazi, E. James, Y. Mehellou, The ProTide prodrug technology: Where next? ACS Med. Chem. Lett. 10 (1) (2019) 2–5.

[17] V. Chudasama, A. Maruani, S. Caddick, Recent advances in the construction of antibody–drug conjugates, Nat. Chem. 8 (2) (2016) 114–119.

[18] A. Alouane, R. Labruère, T. Le Saux, F. Schmidt, L. Jullien, Self-immolative spacers: kinetic aspects, structure–property relationships, and applications, Angew. Chem. Int. Ed. 54 (26) (2015) 7492–7509.

[19] G.M. Dubowchik, R.A. Firestone, L. Padilla, D. Willner, S.J. Hofstead, K. Mosure, J. O. Knipe, S.J. Lasch, P.A. Trail, Cathepsin B-labile dipeptide linkers for lysosomal release of doxorubicin from internalizing immunoconjugates: Model studies of enzymatic drug release and antigen-specific in vitro anticancer activity, Bioconjug. Chem. 13 (4) (2002) 855–869.

[20] R.J. Amir, D. Shabat, Self-immolative dendrimer biodegradability by multi-enzymatic triggering, Chem. Commun. 14 (2004) 1614–1615.

[21] R.V. Gonzaga, L.A. do Nascimento, S.S. Santos, B.A. Machado Sanches, J. Giarolla, E.I. Ferreira, Perspectives about self-immolative drug delivery systems, J. Pharm. Sci. 109 (11) (2020) 3262–3281.

[22] S.C. Jeffrey, J.B. Andreyka, S.X. Bernhardt, K.M. Kissler, T. Kline, J.S. Lenox, R. F. Moser, M.T. Nguyen, N.M. Okeley, I.J. Stone, X. Zhang, P.D. Senter, Development and properties of β-glucuronide linkers for monoclonal antibody−drug conjugates, Bioconjug. Chem. 17 (3) (2006) 831–840.

[23] S.C. Jeffrey, J. De Brabander, J. Miyamoto, P.D. Senter, Expanded utility of the β-glucuronide linker: ADCs that deliver phenolic cytotoxic agents, ACS Med. Chem. Lett. 1 (6) (2010) 277–280.

[24] S. Kolodych, C. Michel, S. Delacroix, O. Koniev, A. Ehkirch, J. Eberova, S. Cianférani, B. Renoux, W. Krezel, P. Poinot, C.D. Muller, S. Papot, A. Wagner, Development and evaluation of β-galactosidase-sensitive antibody-drug conjugates, Eur. J. Med. Chem. 142 (2017) 376–382.

[25] E. Cini, V. Faltoni, E. Petricci, M. Taddei, L. Salvini, G. Giannini, L. Vesci, F. M. Milazzo, A.M. Anastasi, G. Battistuzzi, R. De Santis, Antibody drug conjugates (ADCs) charged with HDAC inhibitor for targeted epigenetic modulation, Chem. Sci. 9 (31) (2018) 6490–6496.

[26] F.M. Milazzo, L. Vesci, A.M. Anastasi, C. Chiapparino, A. Rosi, G. Giannini, M. Taddei, E. Cini, V. Faltoni, E. Petricci, G. Battistuzzi, L. Salvini, V. Carollo, R. De Santis, ErbB2 targeted epigenetic modulation: Anti-tumor efficacy of the ADC trastuzumab-HDACi ST8176AA1, Front. Oncol. (2020) 9.

[27] C. Cianferotti, V. Faltoni, E. Cini, E. Ermini, F. Migliorini, E. Petricci, M. Taddei, L. Salvini, G. Battistuzzi, F.M. Milazzo, A.M. Anastasi, C. Chiapparino, R. De Santis, G. Giannini, Antibody drug conjugates with hydroxamic acid cargos for histone deacetylase (HDAC) inhibition, Chem. Commun. 57 (7) (2021) 867–870.

[28] F. Migliorini, E. Cini, E. Dreassi, F. Finetti, G. Ievoli, G. Macrì, E. Petricci, E. Rango, L. Trabalzini, M. Taddei, A PH-responsive crosslinker platform for antibody-drug conjugate (ADC) targeting delivery, Chem. Commun. 58 (75) (2022) 10532–10535.

[29] C.E. Stieger, Y. Park, M.A.R. de Geus, D. Kim, C. Huhn, J.S. Slenczka, P. Ochtrop, J. M. Müchler, R.D. Süssmuth, J. Broichhagen, M. Baik, C.P.R. Hackenberger, DFT-guided discovery of ethynyl-triazolyl-phosphinates as modular electrophiles for chemoselective cysteine bioconjugation and profiling, Angew. Chem. Int. Ed. 61 (41) (2022).

[30] J.C. Kern, M. Cancilla, D. Dooney, K. Kwasnjuk, R. Zhang, M. Beaumont, I. Figueroa, S. Hsieh, L. Liang, D. Tomazela, J. Zhang, P.E. Brandish, A. Palmieri, P. Stivers, M. Cheng, G. Feng, P. Geda, S. Shah, A. Beck, D. Bresson, J. Firdos, D. Gately, N. Knudsen, A. Manibusan, P.G. Schultz, Y. Sun, R.M. Garbaccio, Discovery of pyrophosphate diesters as tunable, soluble, and bioorthogonal linkers for site-specific antibody–drug conjugates, J. Am. Chem. Soc. 138 (4) (2016) 1430–1445.

[31] M.A. Kasper, P. Ochtrop, A. Jagtap, et al., Expanding the payload scope in antibody-drug conjugates: Unprecedented delivery of hydroxy-containing drugs through self-immolative phosphoramidates, Research Square (2025), https://doi.org/10.21203/rs.3.rs-5454963/v1. PREPRINT (Version 1).

[32] S.D. Gesto, M.F.S.A.N. Cerqueira, A.P. Fernandes, J.M. Ramos, Gemcitabine: A critical nucleoside for cancer therapy, Curr. Med. Chem. 19 (7) (2012) 1076–1087.

[33] M. Slusarczyk, M.H. Lopez, J. Balzarini, M. Mason, W.G. Jiang, S. Blagden, E. Thompson, E. Ghazaly, C. McGuigan, Application of ProTide technology to gemcitabine: A successful approach to overcome the key cancer resistance mechanisms leads to a new agent (NUC-1031) in clinical development, J. Med. Chem. 57 (4) (2014) 1531–1542.

[34] H. Zhong, J. Mu, Y. Du, Z. Xu, Y. Xu, N. Yu, S. Zhang, S. Guo, Acid-triggered release of native gemcitabine conjugated in polyketal nanoparticles for enhanced anticancer therapy, Biomacromolecules 21 (2) (2020) 803–814.

[35] B. Pandit, M. Royzen, Recent development of prodrugs of gemcitabine, Genes (Basel) 13 (3) (2022) 466.

[36] Z. Li, R. Shu, M. Li, X. Wang, X. Chen, H. Chen, X. Wu, J. Chen, Recent progress in gemcitabine-loaded nanoparticles for pancreatic cancer therapy: A review, Nanoscale 17 (30) (2025) 17480–17507.

[37] P.J. Thornton, H. Kadri, A. Miccoli, Y. Mehellou, Nucleoside phosphate and phosphonate prodrug clinical candidates, J. Med. Chem. 59 (23) (2016) 10400–10410.

[38] M.J. Sofia, D. Bao, W. Chang, J. Du, D. Nagarathnam, S. Rachakonda, P.G. Reddy, B.S. Ross, P. Wang, H.-R. Zhang, S. Bansal, C. Espiritu, M. Keilman, A.M. Lam, H.M. M. Steuer, C. Niu, M.J. Otto, P.A. Furman, Discovery of a β-D-2′-Deoxy-2′-α-fluoro-2′-β-*C*-methyluridine nucleotide prodrug (PSI-7977) for the treatment of hepatitis C virus, J. Med. Chem. 53 (19) (2010) 7202–7218.

[39] C. Gardelli, B. Attenni, M. Donghi, M. Meppen, B. Pacini, S. Harper, A. Di Marco, F. Fiore, C. Giuliano, V. Pucci, R. Laufer, N. Gennari, I. Marcucci, J.F. Leone, D. B. Olsen, M. MacCoss, M. Rowley, F. Narjes, Phosphoramidate prodrugs of 2′-*C*-methylcytidine for therapy of hepatitis C virus infection, J. Med. Chem. 52 (17) (2009) 5394–5407.

[40] P. Büchler, H.A. Reber, M.C. Büchler, M.A. Roth, M.W. Büchler, H. Friess, W. H. Isacoff, O.J. Hines, Therapy for pancreatic cancer with a recombinant humanized anti-HER2 antibody (herceptin), J. Gastrointest. Surg. 5 (2) (2001) 139–146.

[41] A. Kokot, S. Gadakh, I. Saha, E. Gajda, M. Łaźniewski, S. Rakshit, K. Sengupta, A. F. Mollah, M. Denkiewicz, K. Górczak, J. Claesen, T. Burzykowski, D. Plewczynski, Unveiling the molecular mechanism of trastuzumab resistance in SKBR3 and BT474 cell lines for HER2 positive breast cancer, Curr. Issues Mol. Biol. 46 (3) (2024) 2713–2740.